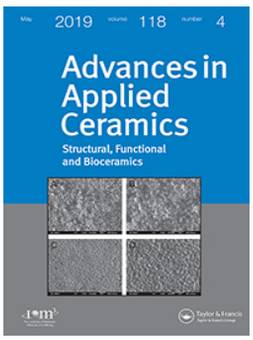

Taylor & Francis
Taylor & Francis Group

Advances in Applied Ceramics

Structural, Functional and Bioceramics

ISSN: 1743-6753 (Print) 1743-6761 (Online) Journal homepage: https://www.tandfonline.com/loi/yaac20

Design and development of ring-on-ring jig for biaxial strength testing of brittle ceramic composite materials: ZrB_2-30wt-%SiB_6

Alejandro Carrasco-Pena, Ryan Jordan, Jessica Dieguez, Arturo Coronado-Rodríguez, Veli B. Ozdemir, Kawai Kwok, Nina Orlovskaya, Demetrius A. Vazquez-Molina, Fernando J. Uribe-Romo, Amy Bolon, Miladin Radovic, Salvatore Grasso & Mike J. Reece

To cite this article: Alejandro Carrasco-Pena, Ryan Jordan, Jessica Dieguez, Arturo Coronado-Rodríguez, Veli B. Ozdemir, Kawai Kwok, Nina Orlovskaya, Demetrius A. Vazquez-Molina, Fernando J. Uribe-Romo, Amy Bolon, Miladin Radovic, Salvatore Grasso & Mike J. Reece (2019) Design and development of ring-on-ring jig for biaxial strength testing of brittle ceramic composite materials: ZrB_2-30wt-%SiB_6, Advances in Applied Ceramics, 118:4, 159-168, DOI: 10.1080/17436753.2019.1613102

To link to this article: https://doi.org/10.1080/17436753.2019.1613102

ADVANCES IN APPLIED CERAMICS
2019, VOL. 118, NO. 4, 159–168
https://doi.org/10.1080/17436753.2019.1613102

The Institute of Materials, Minerals and Mining

Taylor & Francis
Taylor & Francis Group

RESEARCH ARTICLE

Design and development of ring-on-ring jig for biaxial strength testing of brittle ceramic composite materials: ZrB_2-30wt-%SiB_6

Alejandro Carrasco-Pena[a], Ryan Jordan[a], Jessica Dieguez[a], Arturo Coronado-Rodríguez[a], Veli B. Ozdemir[a], Kawai Kwok[a], Nina Orlovskaya[a], Demetrius A. Vazquez-Molina [b], Fernando J. Uribe-Romo [b], Amy Bolon[c], Miladin Radovic [c], Salvatore Grasso[d] and Mike J. Reece[d]

[a]Department of Mechanical and Aerospace Engineering, University of Central Florida, Orlando, FL, USA; [b]Department of Chemistry, University of Central Florida, Orlando, FL, USA; [c]Department of Materials Science and Engineering, Texas A&M University, TX, USA; [d]School of Material Science and Engineering, Queen Mary University of London, London, UK

ABSTRACT

The strength of brittle ceramic materials is typically tested using simple uniaxial compression or by three- or four-point bending techniques. While these methods provide reliable results, they do not depict a realistic characterisation of the load-bearing capacity of structural materials, and a method that involves the application of multiaxial stress is required, such as the ring-on-ring biaxial flexural strength test. In this paper, an in-house ring-on-ring fixture was developed and validated by comparing the experimental and simulated biaxial strength tests of a model ZrB_2-30wt-%SiB_6 ceramic composite. A description of the simulated finite element analysis is provided, and the stress field acting on the sample with maximum principal stress located at the surface under tension at the centre of the ceramic disk is shown.

ARTICLE HISTORY
Received 15 February 2018
Revised 24 April 2019
Accepted 25 April 2019

KEYWORDS
Ring-on-ring; biaxial flexural strength; finite element method; mechanical properties; powder diffraction; Spark plasma sintering; Resonant ultrasound spectroscopy; microstructure

Introduction

Uniaxial strength of brittle ceramic materials is typically tested using either a simple compression technique or a well-developed three- or four-point bending of bar samples. While reliable and consistent information on uniaxial strength of the ceramic materials can be provided with these techniques it is not very often that in real life the materials are exposed to such simple uniaxial loads. In many practical service applications of ceramics, a multiaxial loading occurs where the stress and related strain distributions are very different than those occurring for the cases where materials are loaded uniaxially. However, the multiaxial stress and strain distributions are required in order to estimate reliability, durability and lifetime of the ceramics under real operational conditions. In order to characterise the behaviour of ceramics under multiaxial loading, for example, biaxial loading, different techniques, such as piston-on-three-balls, ball-on-three-balls, ball-on-ring, and ring-on-ring were developed in the past by different research groups [1–5] with many of those techniques adopted as ASTM C1499 or EN 1288-1:2000 standards [5,6]. Figure 1 shows a schematic of the ball-on-three-balls, ball-on-ring, piston-on-three-balls, and ring-on-ring loading using a thin disk sample to perform the test.

While all of these techniques [1–5] calculate the maximum elastic stress in biaxial loading using equations that include a direct proportionality between stress and applied load [3], yet each of the available techniques have different advantages that make them more suitable over the others when they are to be used under specific testing conditions and specific geometries of ceramic specimens. The comparative analysis of ring-on-ring, piston-on-three-balls, and ball-on-ring testing was performed using FEA by Ritter et al. [7]. It was determined that the ring-on-ring loading gives the most accurate measure of strength for the cases when fracture occurs within the loading ring. However, for the ring-on-ring test a flat and parallel surface geometry of the ceramic disk sample is required, as well as relatively strict requirements for the diameter-to-thickness ratio of the disk which allows to control the amount of sample's displacement, ensuring the disk will not flex excessively during testing and the direct proportionality between the applied load and the resulting biaxial stress can still be maintained [8]. The numerical stress analysis of glass plates tested in ring-on-ring geometry showed that the stress magnifications at the loading ring are significant when the plate deflection exceeds one half of the specimen thickness [8]. In addition, the friction between the ceramic sample and loading and supporting rings exists but it is typically ignored in the analysis. Other techniques, such as ball-on-ring or ball-on-three-balls, have also been merited for biaxial testing of ceramics. In the

CONTACT Alejandro Carrasco-Pena alejandro.carrasco@knights.ucf.edu Department of Mechanical and Aerospace Engineering, University of Central Florida, Orlando, FL, USA

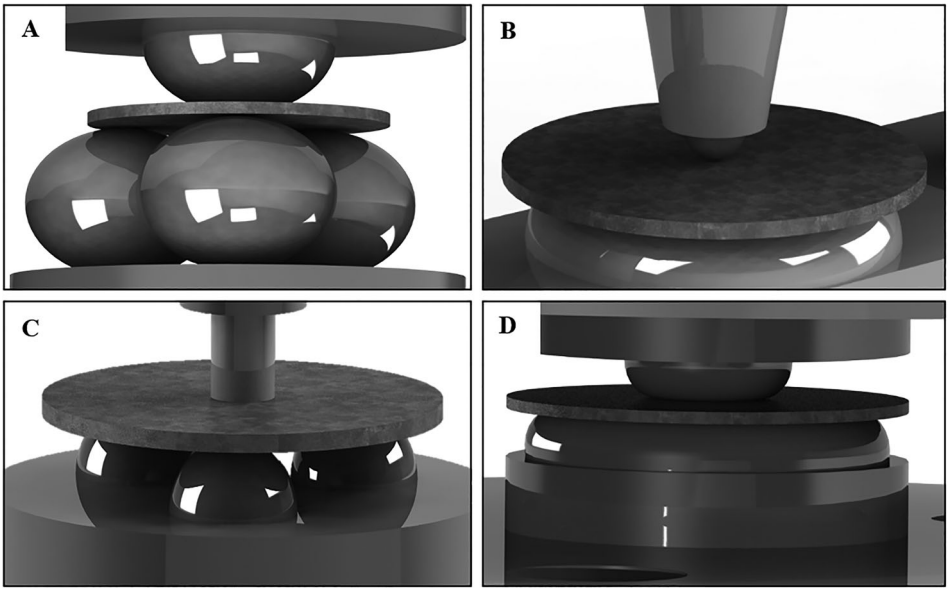

Figure 1. Schematic of biaxial strength tests using ball-on-three-balls (A), ball-on-ring (B), piston-on-three-balls (C), and ring-on-ring (D).

ball-on-ring test the precise knowledge of stresses produced in the sample during loading, combined with an easy alignment of the sample for the test, gives significant advantages for the use of this method. In the ball-on-three-balls test the additional advantage is also considered, when choosing the technique for biaxial tests the requirements for the flatness of ceramic sample are not such stringent as in the case of ring-on-ring or piston-on-three-balls, therefore, sintered samples can be tested without any additional surface preparation. These considerations are important for choosing a specific technique when testing for biaxial strength of ceramics because any deviations that can occur from the sample geometry relationships and parallelism, and its interaction with the testing fixture may introduce different stress distribution and per cent errors that can directly affect the measurements [4]. In order to avoid these uncertainties and errors in the measurement of the biaxial strength, both a jig for biaxial stress tests and the sample geometry has to be designed and developed. The guidelines for the ring-on-ring fixture design and the sample's dimensions can be found in the standard ASTM C1499, where the relationships between sample's geometry and jig dimensions are presented [5]. Owing to the popularity and versatility of the ring-on-ring test its range of application varies from dental material application, such as ceramic dental restorations [9], to the test of biaxial strength for LCD display panels [10] found in today's televisions and cell phones. The ring-on-ring geometry of the biaxial testing jig was adopted as ISO-6474 for orthopaedic alumina and zirconia ceramics. It was also used in the testing of glass [11] as well as ZrO_2 based electrolyte ceramics and other different ceramic materials [12]. In this paper, the design and development of a ring-on-ring jig for testing of brittle ceramic disks is reported. The results of the biaxial strength measurement of ZrB_2-30wt-%SiB_6 ceramic composite chosen as a model material to verify the ring-on-ring jig performance is also presented. In addition to the biaxial strength results, the elastic moduli and Poisson's ratio as well as the estimated stress–strain deformation behaviour of ZrB_2-30wt-%SiB_6 ceramic composites are also reported.

Design and development of the ring-on-ring jig

For the testing of biaxial strength of brittle ceramics at ambient temperature under monotonic loading, the ring-on-ring technique was chosen as the one which would be the most appropriate to test boride based ceramics, such as ZrB_2-30wt-%SiB_6 ceramic composites. The jig developed consists of a support ring, a load ring, a support of the load ring, and a sphere which is used for the specimen's alignment located between the load ring support plate and the load ring itself (Figure 2). The following equation was used for the calculation of the biaxial strength [5],

$$\sigma_f = \frac{3F}{2\pi h^2}\left[(1-\nu)\frac{D_S^2 - D_L^2}{2D^2} + (1+\nu)ln\frac{D_S}{D_L}\right] \quad (1)$$

where F is a fracture load, N; D_S is the support ring diameter, mm; σ_f is the equibiaxial fracture strength, MPa; h is the thickness of the ceramic specimen, mm; ν is the Poisson's ratio; D_L is the load ring diameter, mm. The design of the jig's components was achieved by following the ASTM standard C1499 [5], which strictly depends on the geometry of the ceramic samples to be tested. The following ASTM C1499 relation was used for the calculation of the diameter

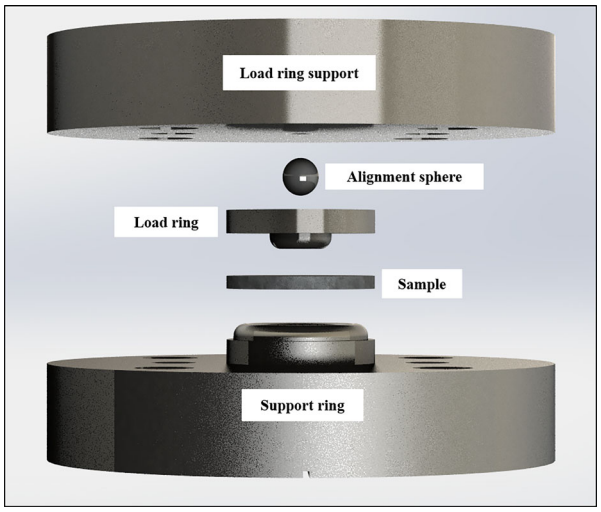

Figure 2. Schematic of the ring-on-ring jig including the sample.

of the support ring,

$$D - 2h \geq D_s \geq D - 12h \tag{2}$$

where D is the diameter of the sample, mm; h is the thickness of the sample, mm; and D_S is the diameter of the support ring, mm. The pre-multiplier 2–12 used in the Equation (2) correlates with the surface finish of the ceramic sample with 12 used for the curved and not flat surfaces, which is the case when samples used in ring-on-ring test are as-sintered without any machining. As the ZrB_2-30wt-%SiB_6 ceramic samples used for the experiments in this paper were machined with diameter varying from 18 to 20.25 mm and thickness varying from 1.03 to 1.42 mm, as found in Table 1, the pre-multiplier was chosen as 3, which yielded a diameter of the support ring, D_S, equal to 15.45 mm. After the calculation of the D_S, the diameter of the load ring was determined using the following relation

$$0.2D_S \leq D_L \leq 0.5D_S \tag{3}$$

where the D_L is the diameter of the load ring, mm. For the D_L the pre-multiplier value was chosen as 0.35 due to the geometry of the sample to be tested and the relationship with D_S. Thus, according to the Equation (3) the diameter of the load ring D_L was calculated to be equal to 5.41 mm. The calculation of the ring tip radius was then done using the equation

$$\frac{h}{2} \leq r \leq \frac{3h}{2} \tag{4}$$

Table 1. Summary of the geometry for the samples used to validate the design of the ring-on-ring jig for the determination of biaxial strength of ceramics.

Sample	Diameter (mm)	Thickness (mm)
1	18.64	1.42
2	19.783	1.06
3	20.25	1.37

where h is the sample thickness, mm; and the r is the load and support ring tip radius, mm. As the r dimension varied from 0.5 to 1.5 h (Equation (4)), a value of $r = 1.58$ mm was chosen. The dimensions for the bleed holes, the bleed slot and the heights of the load and support rings were determined using ASTM Standard load and support fixture designs for equibiaxial testing [5]. The size of the spherical ball located at the notched centre of the top surface of the load ring was determined using the $D_S/12$ relationship. The depth of the notch resulted to be 1.05 mm with an opening that followed two lines separated at 120° from each other which made a circle on the top surface of the notch with a diameter of 3.64 mm. This notch was used as the location of the alignment ball for the load ring. The diameter of the metallic sphere used in the ring-on-ring was of 5 mm. The drawings for the developed load and support rings designed in Solidworks® (Dassault Systèmes, Vélizy-Villacoublay, France), are shown in Figure 3. After the drawings of the ring-on-ring jig components were developed, a 3D printed prototype model was made (Figure 4) using the 3D printer Stratasys® Dimension SST 1200es (Stratasys Ltd., Eden Prairie, Minnesota, U.S.A.), thus allowing to ensure that all dimensions are correct and fit the location of the screw attachments of the MTS Criterion® 43 universal testing machine (MTS Systems Corporation, Eden Prairie, Minnesota, U.S.A.) to be used for biaxial strength tests. After all dimensions were verified and prototyped, the model was installed and tested (Figure 4), then the final version of the ring-on-ring jig was manufactured using 4140 steel which has a HR_C larger than 40. The metallic jig was manufactured using a CNC Fadal® VMC-3016L machine (Fadal Engineering, Brea, California, U.S.A.) due to the high precision that was required for the inner and outer radii of the load and support rings, as well as for the parallelism necessary between the surfaces of the aforementioned components of the jig. The jig components as well as its complete assembly in the MTS Criterion® universal testing machine are shown in Figure 5.

Processing and properties of ZrB_2-30wt-%SiB_6 ceramic compositeZrB_2-30wt-%SiB_6 particulate ceramic composite was chosen as a model material for the biaxial strength testing using the developed ring-on-ring jig. ZrB_2 based ceramic composites are very promising materials for ultra-high temperature applications and their properties have been intensively studied in the past [13]. In order to improve both mechanical properties and oxidation resistance, refractory additives, such as SiC and SiB_6 can be added to ZrB_2 [13–15]. While SiC is an additive of choice for improvement of ZrB_2 ceramics in many publications, in this paper SiB_6 ceramic was chosen as an additive to test the mechanical properties of ZrB_2 based ceramic composites. It was reported that SiB_6 provides an improvement of

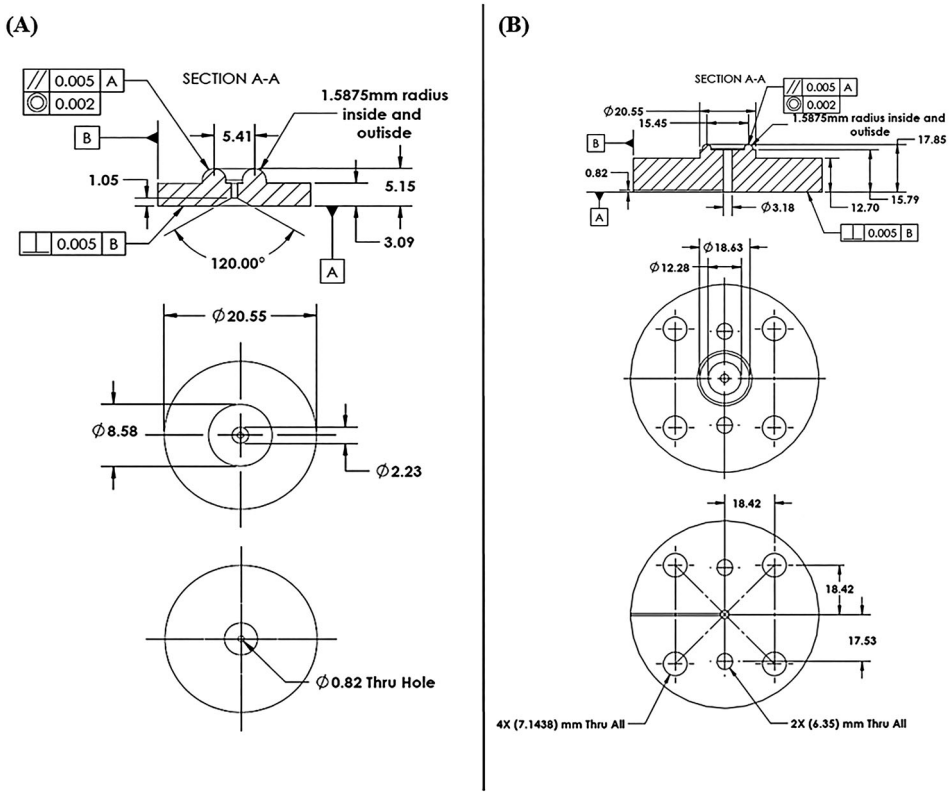

Figure 3. Drawings of the load ring (A) and support ring (B) used for manufacturing of the ring-on-ring jig for biaxial strength testing of brittle ceramic materials.

oxidation resistance of ZrB_2 by the formation of SiO_2 as an oxide protective layer on the surface of the composite at a temperature of 1925°C [15], and it also has a low density and relatively good mechanical properties [16]. The selected properties and lattice parameters of pure ZrB_2 and pure SiB_6 are presented in Table 2 [13–17]. For this study, ZrB_2-30wt-%SiB_6 ceramic composites were used for testing since its biaxial strength has never been studied in the past to the best of the authors' knowledge.

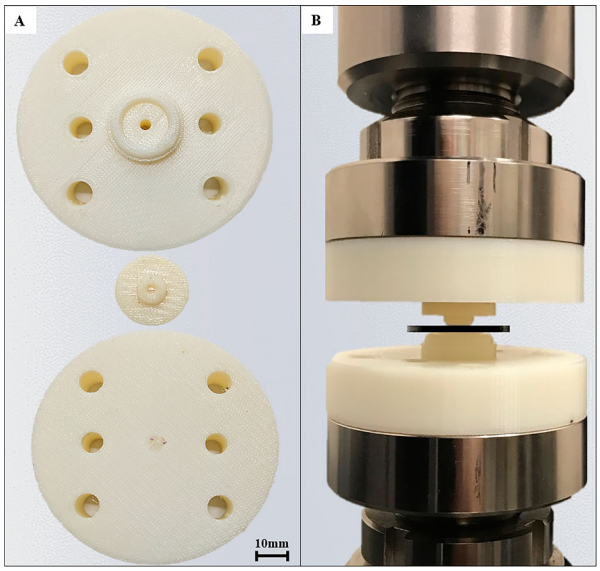

Figure 4. Photographs of the 3D printed prototype of ring-on-ring jig (A) and its assembly in the universal testing machine (B).

Spark plasma sintering of ZrB_2-30wt-%SiB_6 ceramic composite

Spark Plasma Sintering technique (FCT HDP 25; FCT Systeme GmbH, Rauenstein, Germany) was used to sinter a ball milled ZrB_2 (Grade B, H. C. Starck, Goslar, Germany) and SiB_6 (98% pure, −200 mesh, Cerac Inc., U.S.A.) ceramic powders. The graphite die of 20 mm in diameter was packed with the ZrB_2-30wt-%SiB_6 mixed powder and heat up to the sintering temperature of 1750°C and the dwell time of 10 min. The heating rate of 185°C min^{-1} was used to heat up the die to the sintering temperature. After dwell time the machine was switched off and natural cooling was initiated. The temperature, pressure and shrinkage plots collected during SPS of ZrB_2-30wt-%SiB_6 ceramic composite is shown in Table 3 and Figure 6. As one can see, the sintering temperature was 1750°C with the dwell time of 10 min followed by rapid cooling all the way until the die was cooled down to 400°C. From the sintering plot it can be observed when heating was first initiated, but before the pressure was applied, the powder packed in the graphite die expanded resulting in the appearance of positive shrinkage (Zone A on Figure 6). When pressure was applied from zero to 50 MPa the powder was compacted and the significant negative shrinkage appeared (Zone B on Figure 6). However,

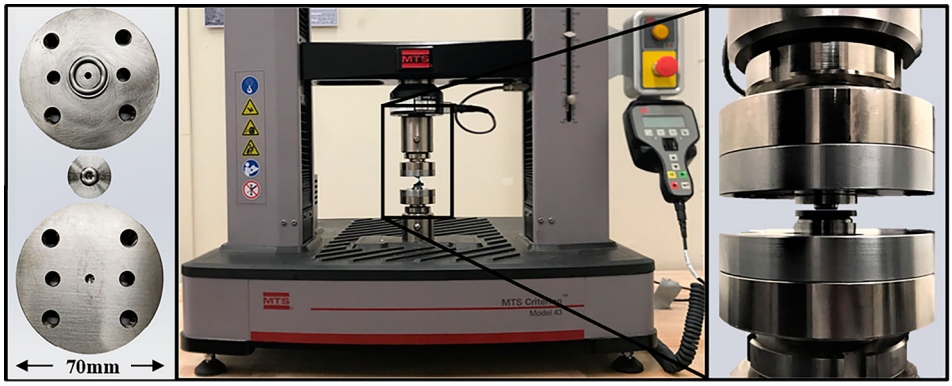

Figure 5. Photographs of the ring-on-ring jig manufactured and mounted on the universal testing machine.

Table 2. Space group, lattice parameters, theoretical density, Young's modulus and Poisson's ratio of ZrB_2 and SiB_6 reported in the literature [13–17].

Property/Parameter	Material	
	ZrB_2	SiB_6
Space group	P6/mmm[13]	Pnnm[16]
Symmetry	Hexagonal[13]	Orthorhombic[16]
a (Å)	3.169[13]	14.397[16]
b (Å)	–	18.318[16]
c (Å)	3.530[13]	9.911[16]
Theoretical density, g cm^{-3}	6.101[14]	2.420[17]
E (GPa)	~ 500[14]	~ 289[15]
v	0.14[14]	–

Table 3. The regions analysed in the SPS sintering plot of the ZrB_2-30wt-%SiB_6 ceramic composite showing the parameters of time, temperature, pressure and displacement presented in Figure 6.

	Time, s	Temperature, °C	Pressure, 10^7 Pa	Shrinkage, mm
A	348	919	142.6	0.11
B	412	1129	448.18	−1.39
C	484	1352	448.18	−1.42
D	614	1750	448.18	−2.15
E	1215	1750	448.18	−3.05
F	1395	942	427.81	−3.79
G	1453	850	101.86	−3.12

this shrinkage was caused only by the applied pressure, as the temperature was still too low (919°C–1129°C) to cause the sintering of the ceramics, therefore, when the 50 MPa pressure was fully applied and remained constant, the further increase on the temperature upon heating caused almost no visible shrinkage in between 1129°C–1352°C temperature (Zone C–D) range, but upon further heating the shrinkage, because of sintering of the powder, was initiated. The most active shrinkage of the composite occurred in between 1352°C–1750°C (Zone C–D in Figure 6) and during the first minute of the dwell time (Zone E in Figure 6). By the end of the dwell time, the shrinkage ended and no further densification could occur (Zone E Figure 6). Upon cooling, the shrinkage occurred due to thermal contraction as temperature decreased (Zone F in Figure 6), however when pressure decreased in Zone G of the plot, the material expanded causing the shrinkage to increase one more time, until it all naturally cooled down with

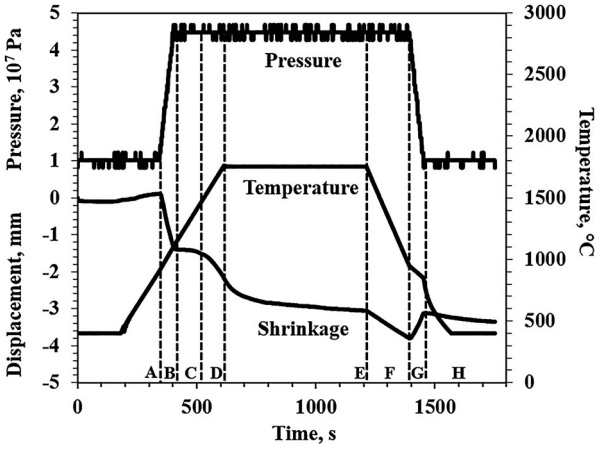

Figure 6. The pressure, temperature, and shrinkage plot showing the sintering parameters of ZrB_2-30wt-%SiB_6 ceramic composite by SPS.

the material shrinking without any applied pressure (Zone H in Figure 6). After sintering, 4.19 g cm^{-3} density of ZrB_2-30wt-%SiB_6 ceramic composite disks was obtained. These ceramic disks were then machined to the diameter of 18 mm and the thickness of 1.7 mm and one of the sides of the machined disks was polished to the mirror surface.

Phase composition and microstructure of ZrB_2-30wt-%SiB_6 ceramic composite

The X-ray diffraction patterns (Rigaku Miniflex 600 diffractometer, Rigaku, Tokyo, Japan) of ZrB_2 and SiB_6 powders used for processing of the composite and ZrB_2-30wt-%SiB_6 ceramic composite bulk material after SPS are shown in Figure 7. Pure single phase diffraction patterns were identified for ZrB_2 and SiB_6 powders. However, while ZrB_2 was retained after SPS as a major phase of the composite, the SiB_6 phase appeared not to be stable, as the peaks clearly belonging to SiB_6 structure [18] were not identified by X-ray diffraction. The Si and B phases were tentatively found instead, indicating the disruption of SiB_6 into two pure compounds. Also, $Si_{11}B_{31}$ phase was also tentatively identified as an existing Si-B compound in the composite,

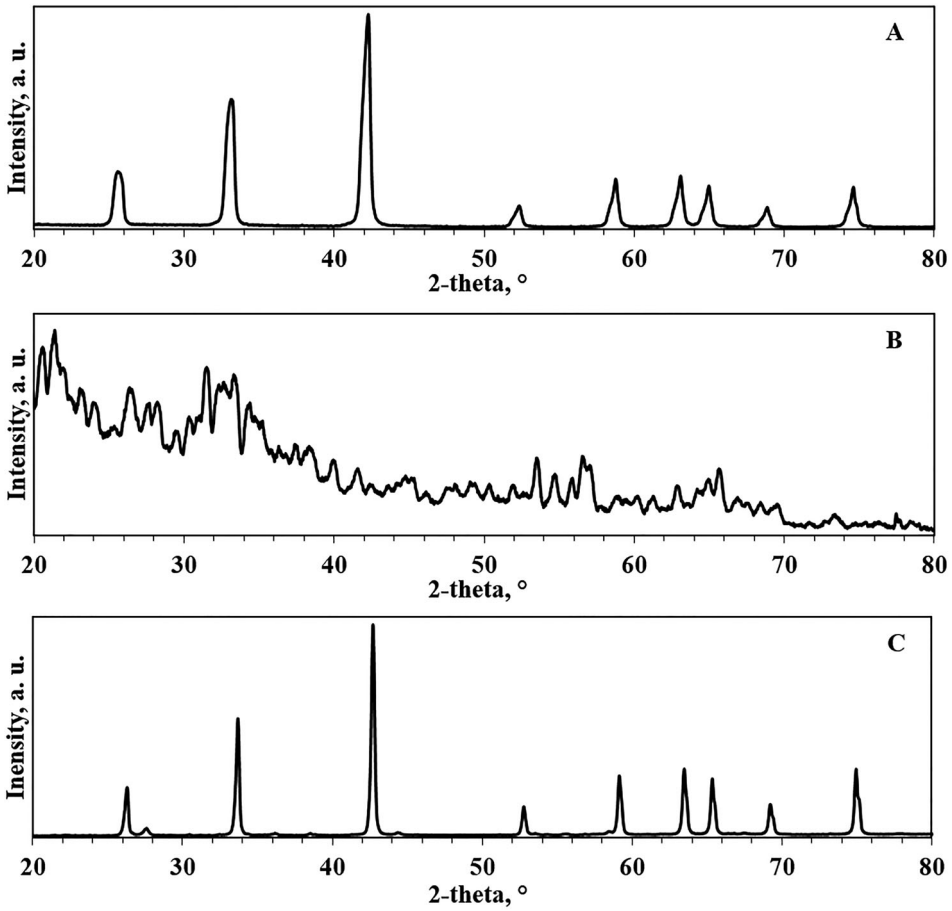

Figure 7. X-ray diffraction patterns of ZrB_2 powder (A), SiB_6 powder (B), and ZrB_2-30wt-%SiB_6 ceramic composite (C).

while a few weak X-ray peaks were not possible to identify at all, thus, the X-ray analysis identified that SiB_6 phase is not a stable phase upon sintering by current assisted SPS technique and a separate study would be required to determine the phase composition of the ZrB_6-SiB_6 ceramic composite after sintering using SPS. However, the composite was still used as a model material to verify the performance of the developed ring-on-ring fixture and further it will be referred as ZrB_2-30wt-%SiB_6.

The microstructure and grain size of ZrB_2-30wt-%SiB_6 ceramic composite was analysed using a Zeiss Axio Lab.A1 (Carl Zeiss AG, Oberkochen, Germany) microscope. The optical micrographs of the ZrB_2-30wt-%SiB_6 ceramic composite are shown in Figure 8. As one can see from the optical micrographs of the ZrB_2-30wt-%SiB_6 microstructure, while in some areas the distribution of the two phases is relatively homogeneous, in many other locations large agglomerations of Si/B phase could be seen. The grain size analysis using intersection method allowed to estimate that the average grain size of ZrB_2 phase was 2.25 μm, while the average grain size of Si/B was 1.90 μm. The grain size distributions of the phases along with their d10, d50, and d90 values are shown in Figure 8. Thus, as one can see from the micrographs and from the grain size analysis the structure is non-homogeneous, which would affect the mechanical performance of this composite.

Mechanical properties of ZrB_2-30wt-%SiB_6 ceramic composite

Elastic properties by resonant ultrasound spectroscopy

The elastic properties of ZrB_2-30wt-%SiB_6 ceramic composite were measured by Resonant Ultrasound Spectroscopy (RUS) (RUSpec, Magnaflux Quasar Systems, Albuquerque, New Mexico) both at room and high temperatures in an Ar protective environment, where the Young's, shear, and bulk moduli along with the Poisson's ratio are shown in Figure 9. The Young's modulus at room temperature was equal to 452 GPa, and shear and bulk moduli were equal to 199 and 210 GPa, respectively. The Poisson's ratio was equal to 0.136 at room temperature [14]. There is almost linear degradation of the elastic moduli with temperature increase where Young's, shear and bulk moduli values are reported to be equal to 418.52, 183.83, and 192.87 GPa at 1000°C, respectively.

Biaxial strength

Three ZrB_2-30wt-%SiB_6 disks were loaded up to failure using the developed ring-on-ring jig. The collected load versus time plot were used to generate the biaxial stress versus time plot shown in Figure 10 where the load was converted into stress using Equation 1. The biaxial strength measured at room temperature for three

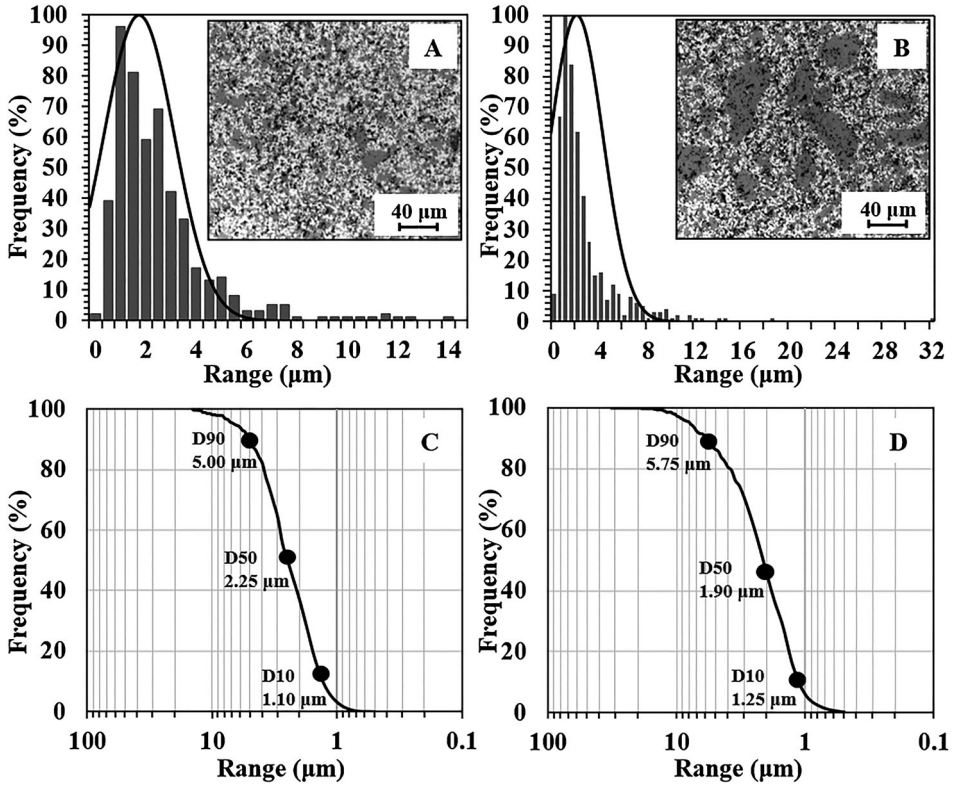

Figure 8. The grain size distribution of ZrB_2 (A) primary phase and Si/B secondary phase (B) with two optical micrographs of the microstructure of the composite showed as inserts.

samples tested was equal to 225.31, 257.90, and 329.85 MPa, which is rather below of the reported uniaxial bending strength of ZrB_2 based ceramic composites, such as 674 ± 130 MPa of 4-point bending strength of ZrB_2-SiC [19] measured at room temperature or 564.72 ± 11.21 MPa of 3-point bending strength of ZrB_2-15vol.-%SiC-15vol.-%$MoSi_2$ [20]. While it is not possible to directly correlate the biaxial strength with the strength values obtained by 4- or 3-point bending techniques, it is still understood that the biaxial strength of ZrB_2-30wt-%SiB_6 ceramic composite is rather low likely because of the decomposition of SiB_6 into different phases during sintering. It is expected that ZrB_2-30wt-%SiB_6 ceramic composites exhibit only elastic behaviour at room temperature, similar to other ZrB_2 based ceramics, as there are not known mechanisms available to introduce the non-linear deformation to the sample tested. Therefore, the generalised Hooke's law was applicable for the recalculation of the ε_x and ε_y strains related to the σ_x and σ_y applied stresses as Young's modulus and Poisson's ratio of the composite was measured by RUS. The estimated stress–strain deformation plots of ZrB_2-30wt-%SiB_6 ceramic composite is also presented in Figure 10.

Finite element analysis simulation of the ring-on-ring test

A finite element (FE) analysis was performed for the ZrB_2-30wt-%SiB_6 samples. It is known that Equation (1) was derived based on linear plate bending theory and the strength calculated is subjected to errors when non-linear geometry effect is significant. The purpose of this analysis was to assess the effect of geometric non-linear deformation in the calculation of strength as well as to validate the results from theory. The FE software used was Simulia Abaqus® 6.19 (Dassault Systèmes, Vélizy-Villacoublay, France). The simulation was run using units of kilograms (kg), millimetres (mm), seconds (s). All interacting parts in the simulation were created in Abaqus® and selected as deformable bodies. Considering the symmetry of the geometry, material properties and loading, a 2D axisymmetric model was created and analysed, thus, a finer mesh control was achieved and more accurate data were observed with minimum computational cost and time. The load- and support-ring were defined as homogeneous elastic using the properties of 4140 steel, while the sample was defined as isotropic linear elastic using the properties obtained experimentally by RUS from the ZrB_2-30wt-%SiB_6 samples. The density used for the 4140 steel and the ZrB_2-30wt-%SiB_6 samples were 7.85 (10^{-6}) kg mm^{-3} and 4.194 (10^{-6}) kg mm^{-3}, respectively, while the elastic modulus and the Poisson's ratio of 4140 steel and the ZrB_2-30wt-%SiB_6 ceramic composite were 200, 452, 0.290, and 0.136 GPa, respectively. The contacts between the load-ring and the sample and the support-ring and the sample were defined as surface-to-surface contacts. Taking into consideration that simulations have been made using frictionless contacts [21] because

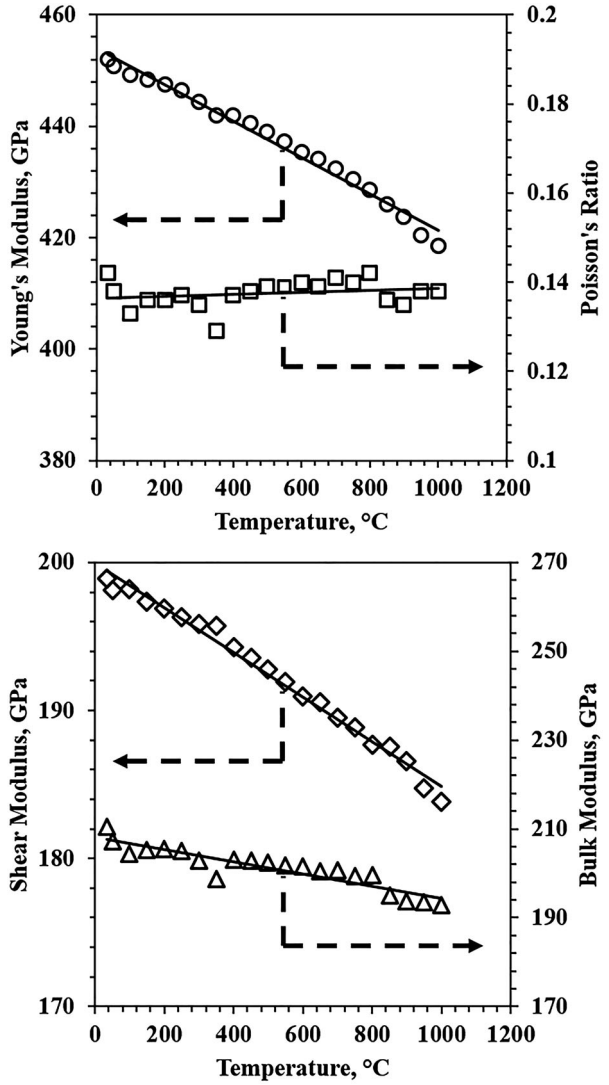

Figure 9. Elastic Properties for ZrB_2-30wt-%SiB_6 measured by RUS. Young's modulus (○), Poisson's ratio (□), shear (◇) and bulk (△) moduli of ZrB_2-30wt-%SiB_6 ceramic composite shown as a function of temperature.

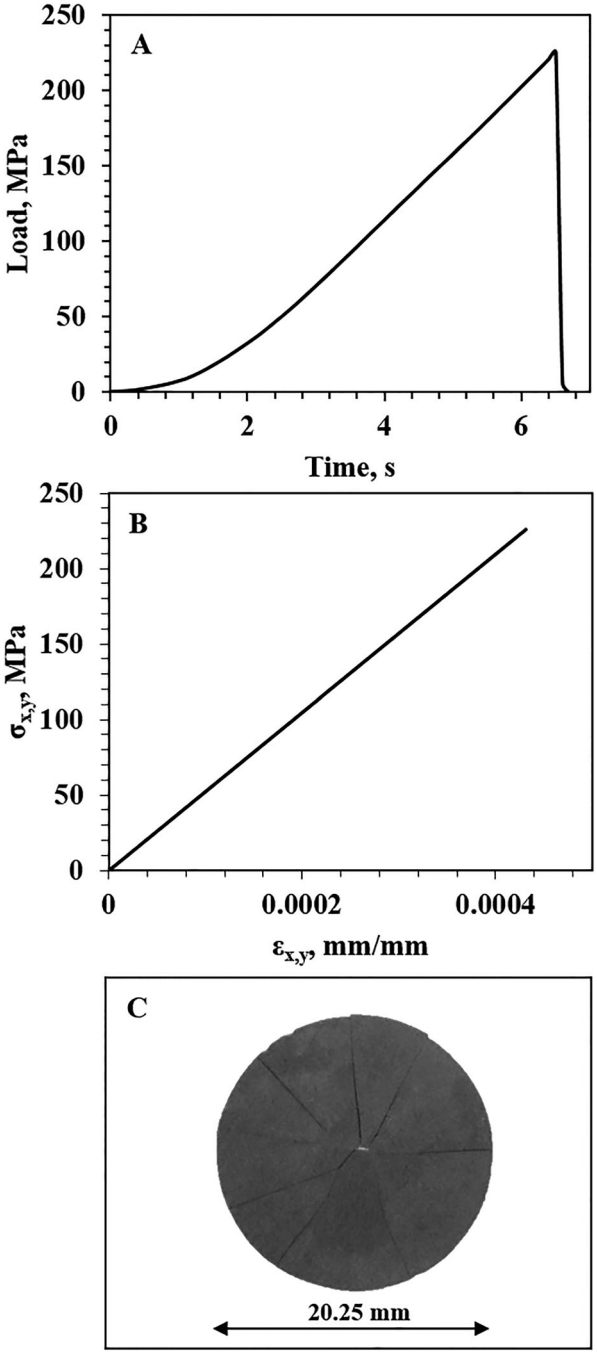

Figure 10. Biaxial stress-time plot (A), stress–strain deformation plot (B) and photograph of fractured sample (C) of ZrB_2-30wt-%SiB_6 ceramic composite disk.

the coefficient of friction in ring-on-ring is very small [5], three runs were made with the same model containing different values for the coefficient of friction, varying from frictionless to 0.1. A static, general step was defined for the simulation with a duration of 6 s with an initial step of 1 s, minimum of 1.00 (10^{-5}) s, and maximum of 6 s. To simulate the behaviour of the interacting elements of the ring-on-ring, the support-ring was fixed in its position by avoiding any displacement or rotation whatsoever; for the load-ring, only *y*-axis displacement was allowed. From the experimental data, the force measured right before the sample broke, 654.82 N, was used to calculate uniform pressure over the load-ring top surface area. A pressure of 12.13 N mm^{-2} resulted and was applied. For the load- and support-ring, a regular mesh with size of 0.1 mm was used, while the sample was meshed with a size of 0.04 mm uniformly over the section, yielding 8155 elements in total for the ceramic disk section. For the load- and support-ring 4-node bilinear axisymmetric quadrilateral, reduced integration, hourglass controlled (CAX4R) were used, and for the sample, 8-node biquadratic axisymmetric quadrilateral (CAX8R) elements were used. From the simulation, it was determined that the maximum tensile biaxial stress occurs inside the load-ring, on the bottom of the disk, indicated by red area in Figure 11, with a value of 224.3, 227.3, and 230.3 MPa, for the runs with coefficient of friction equal to 0.1, 0.05, and frictionless, respectively, which are close to the experimentally measured value of 225.31 MPa. The closest value was obtained with the run involving the coefficient of friction of 0.1, which yielded an error of 0.4482%. Figure 12 shows

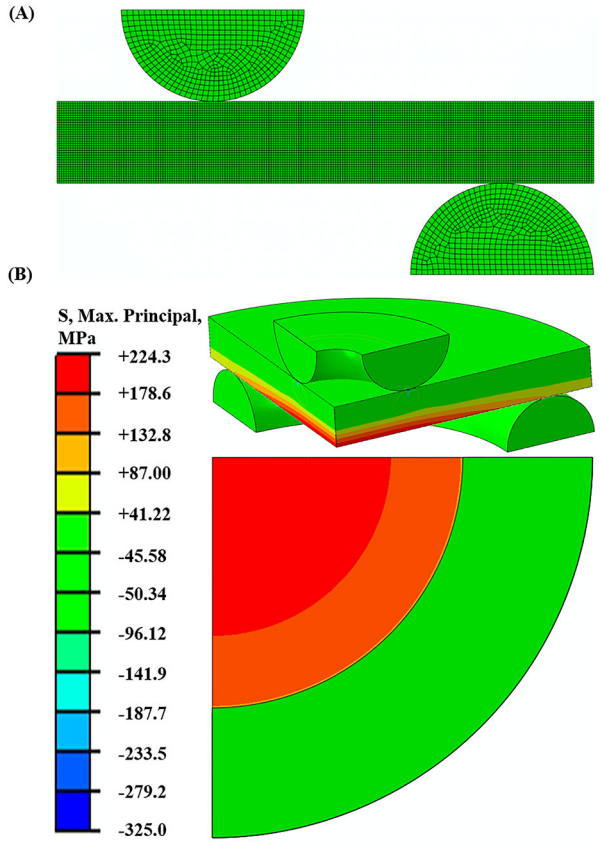

Figure 11. Mesh distribution (A) and FE model of the quarter ring-on-ring test with coefficient of friction of 0.1 showing maximum principal stress for a pressure of 12.13 N mm^{-2} in 6 s (B).

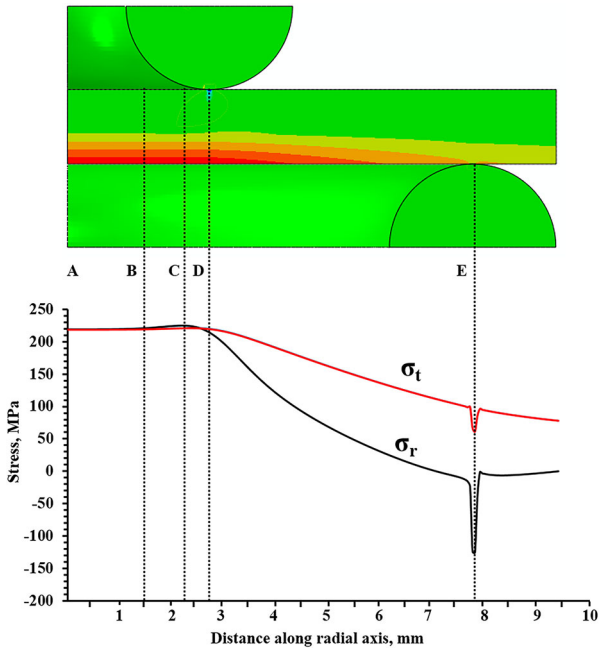

Figure 12. Tangential (σ_t) and radial (σ_r) stress distribution at the bottom tensile surface of the sample disk, shown in the upper portion of the figure, from the centre to the edge of the disk, with coefficient of friction 0.1 and pressure of 12.13 N mm^{-2}.

how the radial, σ_r, and tangential, σ_t, stresses on the tensile surface vary as a function of the radial distance for the simulation with coefficient of friction of 0.1. σ_r and σ_t are equal at the centre of the tensile surface of the disk sample in the region enclosed by the load ring represented by the area marked by *A*-*B* in Figure 12. Vepakomma et al. [10] and Hsueh et al. [21] show that in a ring-on-ring simulation, the variation of maximum principal stress along the radial direction of the tensile surface shows a peak that occurs in the region enclosed by the load ring indicating that the stress is no longer uniform. The same behaviour was found in the simulation developed in this paper where, in Figure 12, σ_r is larger than σ_t for a small region, peaking in the line marked by *C*, and decreasing rapidly as the radial length distances from the centre of the disk. The line marked by *D* in Figure 12 shows the inflection point of σ_t and how it decreases in intensity, not as rapidly as σ_r, when it is measured in distances further from the centre of the sample. The inflection of the curve for the distribution of σ_t aforementioned occurs in a radial distance right below the contact point between the load ring and the sample. The line marked by *E* in Figure 12 shows an outlier point that describes an abrupt drop in the stress distribution on the tensile surface of the sample. This drop is caused by compressive stresses that arise from the contact point between the support-ring and the sample, and it does not represent a critical condition since its value indicates this is not a failure point in the ring-on-ring test.

Conclusions

A ring-on-ring biaxial flexural strength fixture was developed in-house to test the biaxial strength of different disk-shaped ceramic components with diameter and thickness ranging from 18 to 36 and 1.05 to 3.18 mm, respectively. This test was selected due to the simplicity in design and development of the jigs by following the ASTM C-1499 standard. A significant disadvantage of this method is the requirement for flat parallel samples that makes their preparation extensive and time consuming and not permitting for the testing of as-sintered samples. A model ceramic material composed of ZrB_2-30wt-%SiB_6 sintered using SPS technique was used to validate the manufactured ring-on-ring fixture. The X-ray diffraction was used to obtain the phase composition of the model ZrB_2-30wt-%SiB_6 ceramic composite while optical microscopy was used to calculate the grain size distribution. X-ray diffraction analysis showed that the ZrB_2 phase was stable while the SiB_6 phase was non-stable after sintering of the composite. The non-homogeneous phase distribution was measured by optical microscopy showing the appearance of large agglomerates/grains in ZrB_2-30wt-%SiB_6 composite. The RUS was used to measure elastic properties of the composite both at room and high temperature in an Ar protective environment.

The calculation of the biaxial strength was simplified by using simple-plate theory, which only depends on the Poisson's ratio of the material being tested, as specified by the ASTM C1499 standard. The measured values of biaxial strength using ring-on-ring jig were compared to a model developed using the FE method for the elastic region of the ceramic composite assuming a homogeneous material. This FE analysis showed a close correlation to the experimental results from which it can be concluded that the jig designed was validated since the maximum absolute stress occurred in the tensile surface region of the ceramic disk enclosed by the load ring with a value of 224.9 MPa, decreasing gradually as the radius of the disk increases.

Acknowledgement

Dr Yan Chen, Oak Ridge National Laboratory, help with the X-ray analysis of ZrB_2-30wt-%SiB_6 is greatly appreciated.

Disclosure statement

No potential conflict of interest was reported by the authors.

Funding

This research was supported by National Science Foundation (NSF) MRI project '133775' in the United States, NSF REU grant 1461202 awarded to Texas A&M University, and Engineering and Physical Sciences Research Council (EPSRC) [EP/K008749/1, XMat] in the United Kingdom.

ORCID

Demetrius A. Vazquez-Molina http://orcid.org/0000-0003-1986-3028
Fernando J. Uribe-Romo http://orcid.org/0000-0003-0212-0295
Miladin Radovic http://orcid.org/0000-0003-4571-2848

References

[1] Huang CW, Hsueh CH. Piston-on-three-ball versus piston-on-ring in evaluation of the biaxial strength of dental ceramics. Dent Mater. 2011;27:e117–e123.
[2] Borger A, Supancic P, Danzer R. The ball on three balls test for strength testing of brittle discs: stress distribution in the disc. J Eur Ceram Soc. 2002;22:1425–1436.
[3] Shetty DK, Rosenfield AR, McGuire P, et al. Biaxial flexure test for ceramics. Am Ceram Soc Bull. 1980;59(12):1193–1197.
[4] Wendler M, Belli R, Petschelt A, et al. Chairside CAD/CAM materials. Part 2: flexural strength testing. Dent Mater. 2017;33:99–109.
[5] ASTM Standard C1499. Standard test method for monotonic equibiaxial flexural strength of advanced ceramics at ambient temperature. West Conshohocken (PA): ASTM International; 2003; doi:10.1520/C1499-15, www.astm.org.
[6] CEN Standard 1288-1:2000. Glass in building. Determination of the bending strength of glass. Fundamentals of testing glass, The European Standards. 2000. Brussels, ICS: 81.040.20, 1–28.
[7] Ritter JE, Jakus K, Batakis A, et al. Appraisal of biaxial strength testing. J Non Cryst Solids. 1980;38-39 (1):419–424.
[8] Kao R, Perrone N, Capps W. Large-deflection solution of the coaxial-ring-circular-glass-plate flexure problem. J Am Ceram Soc. 1971;54(11):566–571.
[9] Kelly RD, Fleming GJP, Hooi P, et al. Biaxial flexure strength determination of endodontically accessed ceramic restorations. Dent Mater. 2014;30:902–909.
[10] Vepakomma KH, Westbrook J, Carley S, et al. Finite element analysis of ring-on-ring test on LCD panels. J Disp Technol. 2013;9(8):673–677.
[11] Morell R, McCormick NJ, Bevan J, et al. Biaxial disc flexure – modulus and strength testing. Br Ceram Trans. 1999;98(5):234–240.
[12] Chen Y, Aman A, Lugovy M, et al. Residual stress and biaxial strength in Sc_2O_3-CeO_2-ZrO_2/Y_2O_3-ZrO_2 layered electrolytes. Fuel Cells. 2013;13(6):1068–1075.
[13] Pan Y, Zhou B. Zrb_2: Adjusting the phase structure to improve the brittle fracture and electronic properties. Ceram Int. 2017;43:8763–8768.
[14] Lugovy M, Slyunyayev V, Orlovskaya N, et al. Temperature dependence of elastic properties of ZrB_2-SiC composites. Ceram Int. 2016;42:2439–2445.
[15] Clougherty EV, Kalish D, Peters ET. Research and development of refractory oxidation resistant diborides. Technical Report AFML-TR_68-190, Air Force Material Laboratory. 1968:2–4.
[16] Dutta SK, Gazza GE. Properties of hot-pressed SiB_6. Ceramic Bulletin. 1973;52:552–554.
[17] Vlasse M, Slack GA, Garbauskas M, et al. The crystal structure of SiB_6. J Solid State Chem. 1986;63:31–45.
[18] Adamsky R. Unit cell and space group of orthorhombic SiB_6. Acta Crystallogr. 1958;11:744–745.
[19] Orlovskaya N, Stadelmann R, Lugovy M, et al. Mechanical properties of ZrB_2-SiC ceramic composites: room temperature instantaneous behaviour. Adv Appl Ceram. 2013;112(1):9–16.
[20] Li C, Lin Y, Wang M, et al. Preparation and mechanical properties of ZrB_2-based ceramics using $MoSi_2$ as sintering aids. Front Mater Sci China. 2010;4(3):271–275.
[21] Hsueh CH, Luttrell CR, Becher PF. Modelling of bonded multilayered disks subjected to biaxial flexure tests. Int J Solids Struct. 2006;43:6014–6025.